IEEE Access
Multidisciplinary | Rapid Review | Open Access Journal

Received December 4, 2019, accepted January 10, 2020, date of publication January 17, 2020, date of current version January 31, 2020.

Digital Object Identifier 10.1109/ACCESS.2020.2967461

Deep Learning Aided Signal Detection for SPAD-Based Underwater Optical Wireless Communications

RUI JIANG[1], CAIMING SUN[1,2,3], LONG ZHANG[1], XINKE TANG[1], HONGJIE WANG[2], AND AIDONG ZHANG[1,2,3]

[1]Robotics Research Center, Peng Cheng Laboratory (PCL), Shenzhen 518055, China
[2]Institute of Robotics and Intelligent Manufacturing (IRIM), The Chinese University of Hong Kong (CUHK), Shenzhen 518172, China
[3]Shenzhen Institute of Artificial Intelligence and Robotics for Society (AIRS), The Chinese University of Hong Kong (CUHK), Shenzhen 518172, China

Corresponding author: Caiming Sun (cmsun@cuhk.edu.cn)

This work was supported in part by the Collaborative Operation Platform for Smart Underwater Robots (COPSUR) through the PCL Key Project, in part by the Shenzhen Natural Science Foundation under Grant JCYJ20180508163015880, and in part by the National Natural Science Foundation of China under Grant U1613223 and Grant U1813207.

ABSTRACT In underwater optical wireless communication (UOWC) systems, using single photon avalanche photondiode (SPAD) as the detector can improve the transmission distance. However, the signal detection for SPAD-based systems is greatly challenged by the complex optical channel characteristics and SPAD nonlinear distortion. To address this issue, a novel deep learning aided signal detection scheme is proposed in this paper. By exploiting the physical mechanism and prior expert knowledge of the signal processing, a two-connected multilayer perception (MLP) network is integrated into the receiver. The first subnetwork is regarded as a channel compensation block while the second one works as a demodulator. With sophisticated numerical optical channel model and SPAD non-Poisson model, large amounts of training data are utilized to train the proposed model offline. Afterwards, the online data are recovered with the trained network. Simulation results verify that significant bit error ratio (BER) improvement can be achieved with the proposed scheme.

INDEX TERMS Underwater optical wireless communication, nonlinear distortion, deep learning, multilayer perception, signal detection.

I. INTRODUCTION

With the application of technologies such as massive multi-input multi-output transmission, millimeter-wave (mm-mave) communication and non-orthogonal multiple access scheme, 5G mobile communication has significantly increased the system capacity and supported massive connections [1]. However, the 5G network is still ground based [2]. Vast communication demand at sea is greatly challenged due to the limited 5G network coverage. Thus, the envisaged 6G network is expected to provide global wireless connectivity from space to underwater. As a complementary technology for terrestrial communication, optical wireless communication, like laser communication or visible light communication, can be used to support underwater communication and expand the wireless coverage [3].

Underwater optical wireless communication (UOWC) employs the visible light spectrum (mainly the blue-green wavelength) for data transmission. It can provide ultra-high data rate, low time latency and high security [4]. Besides UOWC, underwater acoustic communication and radio frequency (RF) communication can also be used for underwater wireless communication. The underwater acoustic technology is the widely used method for underwater communication in the past decades. It can support long-distance transmission up to several tens of kilometers [5]. However, using sound for the underwater signal transmission is not simple since the acoustic channel is time-varying and space-varing. The extremely low data rate (only Kbps) also limits its application. Compared to the acoustic communication, RF system can provide a higher data rate up to tens of Mbps. As the

The associate editor coordinating the review of this manuscript and approving it for publication was Zinan Wang.

radio wave can easily pass through the air-water interface, the underwater communication and terrestrial communication can be switched over smoothly [6]. The defect of this technology is that the distance is confined in the range of several meters due to the conductivity of the water. In comparison with its two counterparts, UOWC is an extremely competitive approach for underwater wireless communication, which provides a tradeoff between the transmission distance and the data rate. With UOWC technologies, moderate distance in the range of tens of meters can be supported while the data rate can reach up to Gbps [7], [8].

Nevertheless, using optical wireless communication in underwater also faces several challenges. In underwater environment, optical signal suffers from severe water absorption and scattering. The interaction between photons and water molecules or other particulate matters causes that the propagation characteristics of the light beam becomes extremely complicated and varies with different water body. As a result, it is elusive to mathematically describe the underwater optical channel accurately and thereafter so is the signal detection. In spite that Radiative Transfer Equation (RTE) provides a theoretical model to describe the absorption and scattering effect in water, deriving an analytical solution is bristling with difficulties. Besides that, improving the transmission distance from tens of meters to hundreds of meters in UOWC is an another challenging work. Using single photon avalanche photondiode (SPAD) as the detector provides a potential solution. Compared to the conventional avalanche photondiode (APD), SPAD is more sensitive so that a single photon can be detected [9]. However, the dead time contributes to the nonlinearity between the average input photon and the average output voltage. As a result, the photon detection exhibits non-Poisson despite the photons arrival is a Poisson process [10].

To deal with the complexity of the mathematical modeling and overcome the nonlinear distortion of SPAD for signal detection in UOWC, deep learning can be used for this physical-layer communication [11]. As a subbranch of machine learning, deep learning can provide a data-driven method to solve this problem by extracting the feature of large amounts of training data and optimizing the system performance [12]. In such a system, the mathematical model for the processing block is optional and can be replaced by the deep learning network. Although whether the deep learning based wireless communication outperforms the traditional one in terms of the performance improvement and complexity is an open issue, it is believed that the deep learning based algorithm can be executed faster with lower power consumption compared to its counterpart [11].

Recently, the deep learning method has been applied in optical wireless communication to address the physical-layer issues. In [13], a Gaussian kernel-aide deep neural network is applied for 8-pulse amplitude modulation based signal detection to compensate for the nonlinear distortion in an underwater optical system. To mitigate the high peak-to-average power ratio (PAPR) of the optical orthogonal frequency division multiplexing (O-OFDM) based visible light communication system, an autoencoder network is proposed with efficient learning and end-to-end performance optimization [14]. Similar autoencoder network framework is proposed for binary signal designing in LED-based visible light communications [15]. The cost function is deliberatedly designed to satisfy the target dimming constraints. In [16], three demodulators based on convolution neural network, deep belief network and adaptive boosting are compared in a hardware prototype of an end-to-end VLC system with practical datasets.

Against this background, in this paper, a novel deep learning aided signal detection scheme is proposed for SPAD based UOWC system. A two-connected multilayer perceptron (MLP) network as the deep learning architecture is integrated into the signal processing blocks. The first block of the connected MLP network can be regarded as the channel compensation block while the second one works as a demodulator. Compared to existing channel compensation or channel equalization methods, the channel side information is no longer needed for the deep learning aided signal detection. With sophisticated numerical optical channel model and SPAD non-Poisson model, large amounts of training data can be utilized to train the proposed network. Our simulation results show that the deep learning method can address the optical channel distortion as well as SPAD non-Poisson distortion, and thereafter improve the system performance.

The remainder of this paper is organized as follows: In Section II, we describe the characteristics of the UOWC systems, including the inherent optical property, the underwater optical channel and the SPAD nonlinear detection. The deep learning aided signal detection scheme is introduced in Section III. Section IV presents the simulation results to validate our proposed scheme. Finally, the conclusions are drawn in Section V.

II. SYSTEM CHARACTERISTICS

A. INHERENT OPTICAL PROPERTY

The light propagation characteristics in water is quite different from that in the free space since the photons interact with the particles in water more severely and frequently. As is shown in Fig. 1, when the light moves in water, some parts of the incident beam are absorbed in the water and some parts are scattered by the particles. The absorption effect as well as the scattering effect is noticeable in water and would cause the light attenuation.

To mathematically describe these effect, two inherent optical properties of the light are introduced, namely the absorption coefficient $a(\lambda)$ and the scattering coefficient $b(\lambda)$. Then, the attenuation coefficient $c(\lambda)$ can be expressed as

$$c(\lambda) = a(\lambda) + b(\lambda), \tag{1}$$

where λ is the light wavelength. Since we only focus on the performance of the UOWC systems with a specific wavelength, the parameter λ is omitted for brevity herein.

Volume scattering phase function is an another inherent optical property related to the scattering effect. It is defined

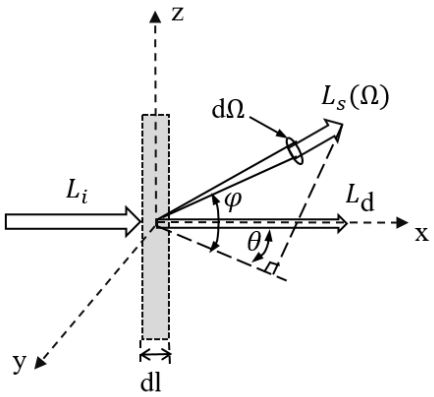

FIGURE 1. Geometry of light propagation in water.

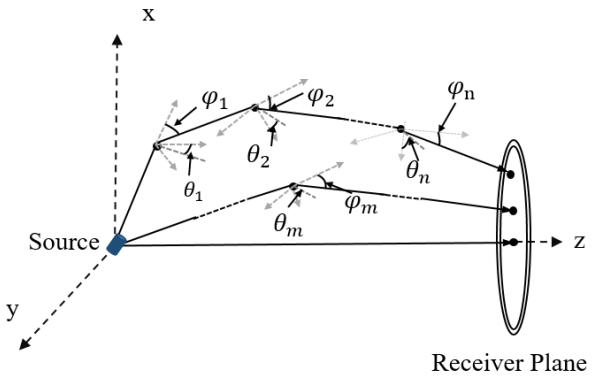

FIGURE 2. Photon propagation trajectory with multiple scattering.

as the proportion of the light scattered out from the incident beam with a solid angle Ω, which is given by

$$\beta(\Omega) = \lim_{dl\to 0}\lim_{d\Omega\to 0}\frac{L_s(\Omega)}{L_i dl d\Omega}, \tag{2}$$

where $L_s(\Omega)$ is the power of the scattered beam toward the solid direction Ω, L_i is the power of the incident beam, $d\Omega$ is the infinitesimal solid angle of the scattered beam and dl is the infinitesimal length of water. Usually, the scattering in the azimuth angle is assumed to be symmetric. Thus, $\beta(\Omega)$ is replaced by $\beta(\varphi)$ for simplicity, where φ is the elevation angle of the scattered beam.

The volume scattering phase function indicates that the scattering in water is non-isotropic and highly forward. Some field experiments have already been done to measure this phase function for the selected realistic water types [17]–[19]. However, these collected data cannot be used directly for theoretical analysis. Thus, several types of analytical models have been proposed. The Henyey-Greenstein phase function is widely used due to its simple expression [20]. Nevertheless, this function is inadequate to represent the realistic light forward scattering at small angle and backscattering at large angle in water. To better describe the realistic light scattering, the two-term Henyey-Greenstein phase function is proposed by summing of two Henyey-Greenstein phase function with different weights [21]. Another more complicated analytical model is the Fournier-Forand marine phase function, which fits well with the Petzold experiment data for San Diego harbor [22].

Based on the volume scattering phase function, the scattering coefficient b is obtained by integrating the volume scattering phase function over all direction (i.e., 4π), which is given by

$$b = \int_0^{4\pi}\beta(\Omega)d\Omega = 2\pi\int_0^{\pi}\beta(\varphi)\sin\varphi d\varphi. \tag{3}$$

By normalizing the volume scattering phase function $\beta(\varphi)$ with the scattering coefficient b, another commonly used function, the scattering phase function $\hat{\beta}(\varphi)$, is obtained to describe the scattering characteristics of the light in water, which is expressed as

$$\hat{\beta}(\varphi) = \frac{\beta(\varphi)}{b}. \tag{4}$$

The scattering phase function can be regarded as the elevation angular distribution probability when photon interacts with the particles in water.

B. UNDERWATER OPTICAL CHANNEL

Based on the attenuation coefficient, the Beer Law is used to model the underwater optical loss, which is formulated as [4]

$$I(L) = I(0)\exp(-cL), \tag{5}$$

where $I(0)$ is the initial radiance of the transmitted light and $I(L)$ is the radiance of the light at the distance L.

The expression of the Beer Law is simple to be used for optical link budget. However, it is not accurate since the photons scattered out of the incident beam are not taken into account when calculating the radiance of the received light. Instead, in consideration of the energy conservation, a more complex but accurate equation, called RTE, is derived to theoretically describe all photons moving through the water along a path toward a given direction. For brevity, the time-independent and source-free RTE can be given by [23]

$$\cos\varphi_2\frac{dI(\varphi_2,\theta_2)}{dl} = -cI(\varphi_2,\theta_2) + \int_0^{\pi}\int_0^{2\pi}\beta\big(\langle\varphi_1,\theta_1\rangle,\langle\varphi_2,\theta_2\rangle\big)I(\varphi_1,\theta_1)\sin\varphi_1 d\theta_1 d\varphi_1. \tag{6}$$

where $I(\varphi_i,\theta_i)$ is the radiance in the direction with the elevation angel φ_i and the azimuth angle θ_i ($i = 1, 2$), $\beta\big(\langle\varphi_1,\theta_1\rangle,\langle\varphi_2,\theta_2\rangle\big)$ is the volume phase scattering function when light is scattered from the direction $\langle\varphi_1,\theta_1\rangle$ into the direction $\langle\varphi_2,\theta_2\rangle$,

Since the equation involves the integrals and derivatives, deriving an exact analytical solution is extremely difficult. Therefore, the Monte Carlo approach has been proposed to numerically evaluate the light radiance when the light passes through water [24]. In this numerical approach, the trajectories of all photons from the light source are simulated. As shown in Fig. 2, each photon would be scattered by the

materials in water for several times. During each scattering time, the photon would change its moving direction randomly. The elevation angle φ_i is generated according to an angular probability based on the scattering phase function while the azimuth θ_i is randomly chosen from $[0, 2\pi]$. Then the new direction cosine $\hat{\mathbf{e}} = [\hat{e}_x\ \hat{e}_y\ \hat{e}_z]^{\mathrm{T}}$ is expressed as

$$\begin{bmatrix}\hat{e}_x\\ \hat{e}_y\\ \hat{e}_z\end{bmatrix} = \begin{bmatrix}\sin\varphi_i\cos\theta_i\\ \sin\varphi_i\sin\theta_i\\ \cos\varphi_i\end{bmatrix} \begin{bmatrix} \frac{e_x e_z}{\sqrt{1-e_z^2}} & \frac{-e_y}{\sqrt{1-e_z^2}} & e_x\\ \frac{e_y e_z}{\sqrt{1-e_z^2}} & \frac{-e_x}{\sqrt{1-e_z^2}} & e_y\\ -\sqrt{1-e_z^2} & 0 & e_z \end{bmatrix}, \quad (7)$$

where $\mathbf{e} = [e_x\ e_y\ e_z]^{\mathrm{T}}$ is the original direction cosine before this scattering event. The photon path length between two scattering events is defined as

$$r_i = -\frac{1}{c}\ln u_i, \quad (8)$$

where u_i is a uniform random number chosen from [0, 1]. Then, the total number of scattering times can be calculated based on the photon path length r_i and the overall distance between the transmitter and the receiver. In addition, the photon would also lose some weights during each scattering time due to the interaction with other particles in water. The photon weight w_i after i times of scattering is given by

$$w_i = \alpha^i w_0, \quad (9)$$

where w_0 is the initial photon weight and α is the single-scattering albedo, which is defined as the ratio of the scattering loss to the attenuation loss. Ultimately, only the photons with the weights above a threshold arriving at the receiver plane from multi-path would be recorded to calculate the received light radiance.

The Monte Carlo approach gives us a numerical underwater optical channel model. In this model, the channel impulse response varies greatly with different water types, link distance and receiver characteristics. Nevertheless, in most cases, the channel time dispersion can be neglected. Even when the light travelling distance is very long and the water is turbid, the maximum delay is less than 12 ns [25]. Thus, the signal suffers from low inter-symbol interference.

C. SPAD NONLINEAR DETECTION

Compared to APD, SPAD has higher sensitivity and can detect single photon as a photon counting receiver. It is useful for signal detection in long distance transmission or low optical power scenarios. SPAD is working in Geiger-mode that an APD is biased with an excess bias voltage above the breakdown voltage. When a photon arrives at the SPAD, an avalanche can be triggered. This avalanche event reduces the SPAD voltage below the breakdown voltage. Before detecting a second photon, SPAD has to be recharged till its voltage is raised to the original bias level with the quenching circuits. This period between the starting of the avalanche event and the recovery of the bias voltage is called as the dead time. Typically, there are two types of quenching circuits configuration that have an impact on the dead time, namely the active quenching (AQ) circuits and the passive quenching (PQ) circuits. For an AQ SPAD, with the use of the AQ circuit, SPAD would be recharged rapidly to the original bias level even when SPAD is fired by another photon in the recharge process. As a result, the dead time would keep constant. While for a PQ SPAD, it can still be triggered by another photon as if the SPAD voltage is above the breakdown voltage. In other words, anther photon arriving during the recharge process can paralyze the device and extend the dead time.

Note that the photon arriving can be modeled as a Poisson process. The probability of detecting k photons can be expressed as

$$P_{\mathrm{ideal}}(k) = \frac{(\lambda_p T)^k e^{-\lambda_p T}}{k!}, \quad (10)$$

where T is the counting interval and λ_p is the average photon arrival rate. In this situation, the average detected photon is $E_{\mathrm{ideal}}(k) = \lambda_p T$, which is proportional to the average photon arrival rate λ_p.

When the dead time is considered, the photon detection no longer follows the Poisson distribution. Typically, the dead time τ is smaller than the counting interval T. If a photon is detected at the start of a counting interval, the maximum number of the counted photons would be $k_{\max} = \lfloor \frac{T}{\tau} \rfloor + 1$, where $\lfloor x \rfloor$ denotes the maximum integer smaller than x.

For an AQ SPAD, its probability of the detected photon is given by [10]

$$P_{\mathrm{AQ}}(k) = \begin{cases} \sum_{i=0}^{k} \frac{\lambda_p^i (T-(k+1)\tau)^i}{i!} e^{-\lambda_p(T-(k+1)\tau)} \\ \quad - \sum_{i=0}^{k-1} \frac{\lambda_p^i (T-k\tau)^i}{i!} e^{-\lambda_p(T-k\tau)}, & \text{if } k < k_{\max}, \\ 0, & \text{if } k \geq k_{\max}. \end{cases} \quad (11)$$

Then the average detected photon is given by

$$E_{\mathrm{AQ}}(k) = (k_{\max}-1) - \sum_{k=0}^{k_{\max}-2} \sum_{i=0}^{k} \frac{\lambda_p^i (T-(k+1)\tau)^i}{i!} e^{-\lambda_p(T-(k+1)\tau)}. \quad (12)$$

While for a PQ SPAD, the probability of the detected photon is given by [10]

$$P_{\mathrm{PQ}}(k) = \begin{cases} \sum_{i=k}^{k_{\max}} (-1)^{i-k} \frac{\lambda_p^i (T-i\tau)^i}{k!(i-k)!} e^{-i\lambda_p\tau}, & \text{if } k < k_{\max}, \\ 0, & \text{if } k \geq k_{\max}. \end{cases} \quad (13)$$

Then the average detected photon is given by

$$E_{\mathrm{PQ}}(k) = \lambda_p e^{-\lambda_p\tau}(T-\tau). \quad (14)$$

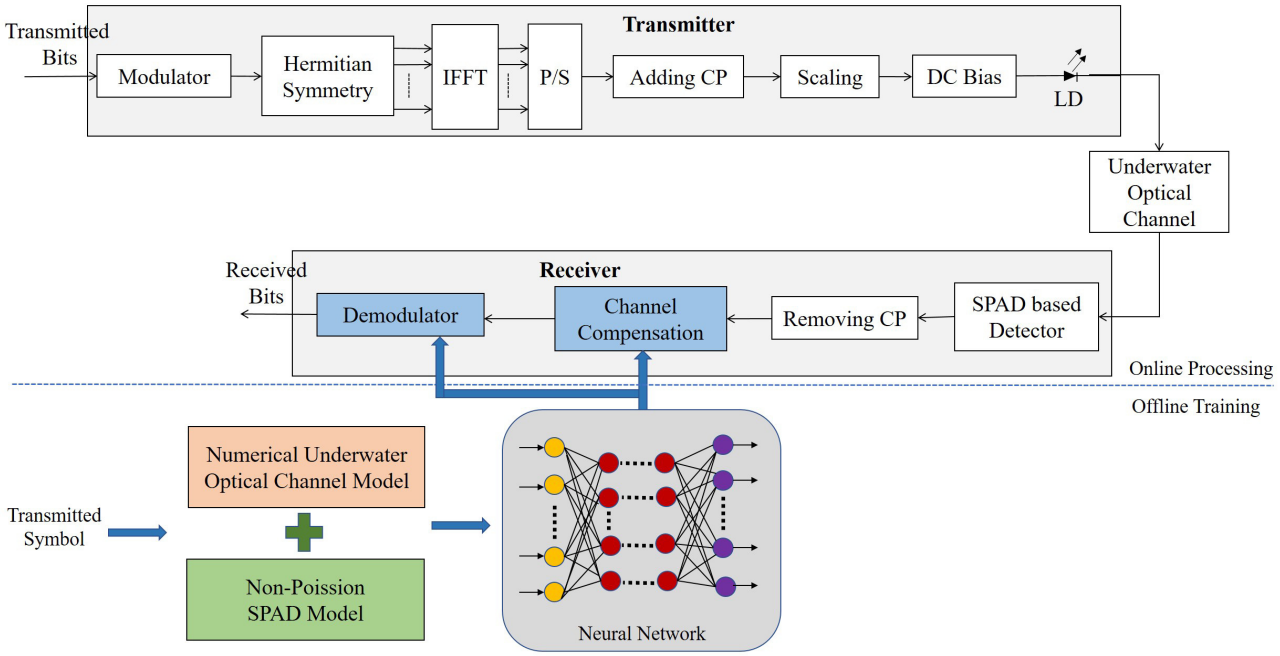

FIGURE 3. Deep learning aided SPAD based UOWC system framework.

From (12) and (14), it can be observed that the dead time could cause the nonlinearity between the arrived photons and the detected photons. To mitigate this nonlinear impact of the dead time, a SPAD array with multiple elements can be used. When photons arrive at the SPAD array, some elements would be triggered while others are still active for another photon detection. However, due to the limited number of the elements in the array, the nonlinearity cannot be eliminated completely [9].

III. SYSTEM DESIGN

In traditional wireless communications, processing blocks such as modulation, channel estimation and channel equalization rely on the mathematically expressed models. However, in some practical scenarios, the interaction between the signal and the environment becomes extremely complex and establishing such mathematical models are intractable [26], [27]. Combining the deep learning with the mature existed mathematically expressed model or associated algorithm for processing block can boost the intelligent communication and achieve comparable performance gains [28]. In this section, a novel signal detection scheme is proposed where the MLP network is integrated into the SPAD based UOWC system with direct current biased optical orthogonal frequency division multiplexing (DCO-OFDM) employed for signal modulation. Among various deep learning network architectures, such as MLP network, convolutional neural network (CNN), recurrent neural network (RNN) and others built upon them, the MLP network is adopted in our work. This is because applying MLP network into signal processing can achieve comparable system performance compared with the CNN network and RNN network but with lower computational time [29]. Besides, the architecture of MLP network is simple and easy to be trained compared to the RNN network where the gradient vanishing problem is hard to deal with [30].

A. SPAD BASED UOWC SYSTEM WITH DCO-OFDM MODULATION

The block diagram of the SPAD based UOWC system is illustrated in Fig. 3. Here, the DCO-OFDM modulation scheme is considered due to its high spectrum efficiency. Specifically, the transmitted bits z_i are firstly modulated with quadrature amplitude modulation (QAM). As UOWC systems usually adopt the intensity modulation/direct detection (IM/DD) scheme, the transmitted signal must be real-valued. Accordingly, the modulated complex symbols X_k follows Hermitian symmetry, which is expressed as

$$X_k = X^*_{N-k}, \quad k = 0, 1, \ldots, N/2 - 1, \tag{15}$$

where the subcarriers X_0 and $X_{N/2}$ are set to zero. The time-domain OFDM signal x_n is obtained with inverse fast Fourier transformation (IFFT) from the modulated symbols X_k, which is given by

$$\begin{aligned} x_n &= \frac{1}{\sqrt{N}} \sum_{k=0}^{N-1} X_k e^{j\frac{2\pi}{N}nk} \\ &= \frac{1}{\sqrt{N}} \sum_{k=1}^{\frac{N}{2}-1} \left[X_k e^{j\frac{2\pi}{N}nk} + X^*_k e^{-j\frac{2\pi}{N}nk} \right] \\ &= \frac{1}{\sqrt{N}} \sum_{k=1}^{\frac{N}{2}-1} \mathrm{Re}\left(X_k e^{j\frac{2\pi}{N}nk} \right), \quad n = 0, 1, \ldots, N-1, \end{aligned} \tag{16}$$

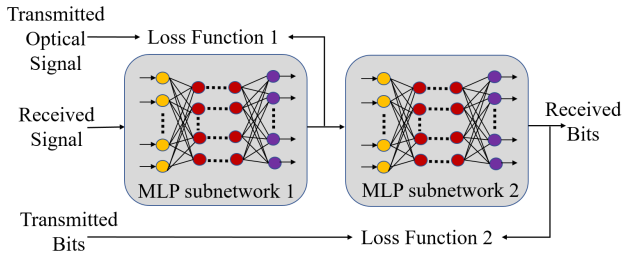

FIGURE 4. Architecture of the proposed two-connected MLP network.

where Re(a) denotes the real parts of a complex symbol a. A cyclic prefix (CP) is then added in front of each OFDM signal to avoid ISI. The time-domain signal x_n is scaled to utilize the dynamic range of the transmitter and satisfy the target power budget. Since the signal should be non-negative, a DC bias is added to the scaled signal before being converted to the optical signal $x_n^{(\text{opt})}$.

At the receiver, to increase the link distance, SPAD is used as the photon detector. The received signal can be expressed as

$$y_n = g_2(g_1(x_n^{(\text{opt})})) \tag{17}$$

where $g_1(\cdot)$ denotes the underwater optical channel distortion and $g_2(\cdot)$ denotes the SPAD nonlinear distortion.

Conventionally, after removing CP, fast Fourier transformation (FFT) is conducted to obtain the frequency symbols from the sampled data. The frequency symbols are sequently equalized and demodulated to recover the original information. Unlike this traditional method, in this paper, a two-connected MLP network is applied to the signal detection by employing the features of the received signals suffering from the distortion of the underwater optical channel and the detector.

It should be mentioned that in machine learning, the training data have a great impact on the performance of the deep learning network and finding such high-quality training data is tricky. Fortunately, obtaining a dedicated training set for network training is much easier in the field of wireless communications since there are many sophisticated models to generate simulated data that match the practical data well, especially in the physical layer. In our scheme, the numeric underwater optical channel model and non-Poisson SPAD model detailed in the previous section are adopted for data generation.

B. DEEP LEARNING AIDED SCHEME

The architecture of the two-connected MLP network is illustrated in Fig. 4. Instead of using one MLP network, two MLP subnetworks are connected intuitively motivated by the signal processing model to improve the training accuracy and reduce the complexity. The first subnetwork of the connected MLP network can be regarded as the channel compensation block while the second one can be regarded as a demodulator. Compared to existing channel compensation or channel equalization methods, the channel side information is no longer needed for the deep learning aided scheme. The loss functions used here to train the network are detailed in the next subsection.

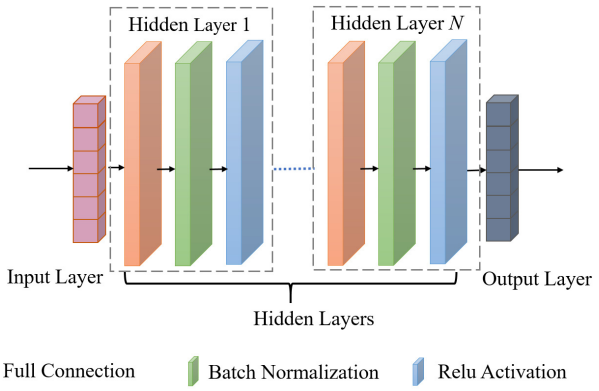

FIGURE 5. Inner structure of the MLP subnetwork.

The inner structure of each subnetwork is further shown in Fig. 5. Each subnetwork consists of one input layer, multiple hidden layers and one output layer. The input layer is the first layer of the MLP subnetwork. Its input is the training data. The last layer of the subnetwork is the output layer which output the data that approaches the expected value. The hidden layers are some special layers where the network does not indicate the exact form or value should be output. They are just used to extract the features of the signals and find the inner connection among them. The output of the previous layer is also the next input of the next hidden layer. Accordingly, the output of each subnetwork can be expressed as

$$\hat{s}_n = f_{N_l}(f_{N_l-1}(\cdots f_1(u_n))), \tag{18}$$

where u_n denotes the input data, N_l denotes the number of layers and the function $f_i(i = 1, 2, \cdots, N_l)$ denotes the nonlinear operation in each layer. Specifically, the nonlinear operation is constituted of three steps, which are the full connection, batch normalization and activation. For a layer l with P_l inputs units and Q_l output units, the full connection among them can expressed as

$$\hat{h}_{l,q} = \sum_{p=1}^{P_l} w_{l,p,q} h_{l,p} + b_{l,q}, \tag{19}$$

where $h_{l,p}$ is the p-th input of layer l, $\hat{h}_{l,q}$ is the q-th output of layer l, $w_{l,p,q}$ is the weights between the p-th input and the q-th output, and $b_{l,q}$ is the bias. It should be pointed out that $\hat{h}_{l,q}$ is not the final output value in this layer. Since gradient exploding and vanishing are two serious problems in the MLP network, batch normalization is applied to address this issue before outputting the final results [31]. It can prevents small weights variation from dramatically amplifying and control the variation of this layer independent of all sequent layers as the data goes through the network, which can be further

expressed as

$$\bar{h}_{l,q} = \gamma_{l,q} \frac{\hat{h}_{l,q} - \mu_{l,q}}{\sqrt{\sigma_{l,q}^2 + \eta}} + \beta_{l,q}, \tag{20}$$

where $\mu_{l,q}$ and $\sigma_{l,q}^2$ denote the mean and variance of the output of q-th neuron in layer l, respectively. $\gamma_{l,q}$ and $\beta_{l,q}$ denote two parameters to be learned, which guarantee that the mean and variance of $\bar{h}_{l,q}$ only depend on this layer. η is a small constant.

Next, the activation function is introduced to obtain the final output of this layer. There are two kinds of activation functions to be used in our proposed network. The first activation function is the relu function, which is used in all hidden layers and given by

$$\sigma_{\text{relu}}(\bar{h}_{l,q}) = \max(0, \bar{h}_{l,q}), \quad l = 1, 2, \cdots, N_l - 1. \tag{21}$$

The second one is the sigmoid function, which is used in the output layer and expressed as

$$\sigma_{\text{sigmoid}}(\bar{h}_{N_l,q}) = \frac{1}{1 + e^{-\bar{h}_{N_l,q}}}. \tag{22}$$

C. OFFLINE TRAINING

Generally, the purpose of offline training of neural network is to reduce the loss function by optimizing the parameters of the MLP network. Here, the mean square error is adopted as the loss function, which is defined as

$$l = \frac{1}{n} \sum_{i=1}^{n} (\hat{s}_n - s_n)^2, \tag{23}$$

where s_n is the expect value. The loss function measures the difference between the actual output of MLP network and the expected output. Since two MLP subnetworks serve as different functions, their expected values are distinct. The expected output of the first block is the transmitted optical signal whereas the expected output of the second one is the transmitted bit.

The training procedure of the deep learning aided signal detection is summarized in Algorithm 1. The first MLP subnetwork is trained with the back-propagation method, which involves the gradient descent algorithm [32]. There are different kinds of gradient algorithms applied into deep learning network. Since the learning rate determines the converging rate of the deep learning network, a self-adaptive learning rate algorithm, called Adam algorithm, is used in our offline training [33]. Adam algorithm exploits the exponential moving averages of the gradient and the squared gradient to scale the learning rate. The weights and bias are updated by

$$\begin{aligned} w_{l,p,q}^{[k]} &\leftarrow w_{l,p,q}^{[k-1]} - \epsilon \frac{m_{l,p,q}^{[k]}}{\sqrt{n_{l,p,q}^{[k]}} + \delta}, \\ b_{l,q}^{[k]} &\leftarrow b_{l,q}^{[k-1]} - \epsilon \frac{\hat{m}_{l,p,q}^{[k]}}{\sqrt{\hat{n}_{l,p,q}^{[k]}} + \delta}, \end{aligned} \tag{24}$$

Algorithm 1 Deep Learning Aided Signal Detection Training Algorithm

Input: For each subnetwork, the length of the input, the number of hidden layers, the number of hidden units in each hidden layer, the length of output, training iteration $N_{\text{nn1,ite}}$, $N_{\text{nn2,ite}}$

1 Start the underwater emulator with the numerical underwater optical channel model and the non-Poisson SPAD model to generate the training data;
2 Normalize the training data;
3 Initial the first MLP subnetwork. The iteration is initially to be 0, and randomly generate the weights and bias;
4 **for** $k = 1$ *to* $N_{nn1,ite}$ **do**
5 Calculate the output of the first MLP subnetwork based on (18);
6 Calculate the loss function between the output of this subnetwork (i.e., $\hat{x}_n^{(\text{opt})}$) and the transmitted optical signal: $l_1 = \frac{1}{N_1} \sum_{n=1}^{N_1} (\hat{x}_n^{(\text{opt})} - x_n^{(\text{opt})})^2$;
7 Update the weights and bias with Adam algorithm based on (24);
8 **end**
9 Initial the second MLP subnetwork while retaining the structure and parameters of the first subnetwork. The iteration is initially to be 0, and randomly generate the weights and bias of this subnetwork ;
10 **for** $k = 1$ *to* $N_{nn2,ite}$ **do**
11 Calculate the output of the second MLP subnetwork based on (18);
12 Calculate the loss function between the output of this subnetwork (i.e., $\hat{z}_i$) and the transmitted bits: $l_2 = \frac{1}{N_2} \sum_{i=1}^{N_2} (\hat{z}_i - z_i)^2$;
13 Update the weights and bias with Adam algorithm based on (24);
14 **end**

where $m_{l,p,q}^{[k]}$ and $n_{l,p,q}^{[k]}$ are the bias-corrected first and seconde raw moment estimate of the mini-batch partial derivation of loss function with respect to the weight $g_w^{[k]}$ in the k-th iteration. Correspondingly, $\hat{m}_{l,p,q}^{[k]}$ and $\hat{n}_{l,p,q}^{[k]}$ are the bias-corrected first and seconde raw moment estimate of the mini-batch partial derivation of loss function with respect to the bias $g_b^{[k]}$. They can be updated by

$$\begin{aligned} m_{l,p,q}^{[k]} &\leftarrow \frac{\alpha_1 m_{l,p,q}^{[k-1]} + (1 - \alpha_1) g_w^{[k]}}{1 - \alpha_1^k}, \\ n_{l,p,q}^{[k]} &\leftarrow \frac{\alpha_2 n_{l,p,q}^{[k-1]} + (1 - \alpha_2)(g_w^{[k]})^2}{1 - \alpha_2^k}, \\ \hat{m}_{l,p,q}^{[k]} &\leftarrow \frac{\alpha_1 \hat{m}_{l,p,q}^{[k-1]} + (1 - \alpha_1) g_b^{[k]}}{1 - \alpha_1^k}, \\ \hat{n}_{l,p,q}^{[k]} &\leftarrow \frac{\alpha_2 \hat{n}_{l,p,q}^{[k-1]} + (1 - \alpha_2)(g_b^{[k]})^2}{1 - \alpha_2^k}. \end{aligned} \tag{25}$$

Here, ϵ, δ, α_1 and α_2 are predefined hyperparameters.

After the first MLP subnetwork is trained, the paraments and its structure is retained. The second MLP subnetwork is then trained with the same method. Once the training of the two subnetworks is completed, the whole network structure with its trained parameters are embedding into the receiver. In the online processing procedure, the received signal is fed to the MLP network. With simple mathematical calculation, the original information can be recovered in a forward propagation manner.

IV. PERFORMANCE EVALUATION

In this section, some simulation results are carried out to test the performance of the proposed scheme. The clear ocean and coastal water are chosen as two typical homogeneous water types. Their absorption, scattering and attenuation coefficients are given in Table 1. The dominant background noise is the dark count noise while the noise from the ambient light is not considered in the simulation. In the optical communication system configuration, a commercial laser diode with the maximum optical power of 85 mW is used at the transmitter while a SPAD array with 64 elements is adopted as the photon detector. For each SPAD element, the dead time is 5 ns. Besides, a 4-QAM based DCO-OFDM with 16 subcarriers is utilized to modulate the transmitted information. The sampling rate for the DCO-OFDM symbol at the receiver is set as 10 MHz. Correspondingly, the photon counting interval is 100 ns and the maximum number of counted photons in a single SPAD element is 21 during a photon counting interval. The specifical photon number in each SPAD element is then generated with the non-Poisson SPAD model (i.e., (11) or (13)). Therefore, the detected photons for each signal sample can be obtained by summing up the detected photons from each SPAD element. In addition, the photon energy for blue light is 4.42×10^{-19} J, which is used for calculating the photon arrival rate for a specific received optical power. Other related parameters used in the simulation are listed in Table 2.

In the MLP network configuration, as the subnetworks work as different signal processing blocks, the number of neurons in their hidden layers are different. In the first subnetwork, there are two hidden layers. The neurons in each layer are 512 and 256, respectively. As the first subnetwork is used for channel compensation, the number of its input data and output data are the same, which equal the number of subcarriers in a DCO-OFDM symbol (i.e., 16). On the other hand, for the second subnetwork, there are two hidden layers with 64 neurons in each layer. Since its input is the output of the first subnetwork, the number of the input data is also 16. The number of its output is set as 14 since the transmitted bits are modulated only on the half of subcarriers of a DCO-OFDM symbol except for the subcarriers X_0 and $X_{N/2}$. It should be mentioned that the achieved BER is unacceptable with the same number of hidden layers and neurons (i.e., 4 hidden layers with 512, 256, 64 and 64 neurons, respectively) in only one MLP network for data training.

TABLE 1. Parameters for typical water types.

Water Type	Absorp. Coeff. (m^{-1})	Scatt. Coeff. (m^{-1})	Attenu. Coeff. (m^{-1})
Clear Ocean	0.037	0.114	0.151
Coastal Water	0.179	0.219	0.398

TABLE 2. Simulation parameters of UOWC systems.

Parameters	Values
Light wavelength	450 nm (blue light)
Modulation scheme	DCO-OFDM with 4-QAM
Number of Subcarriers	16
Photon counting interval	100 ns
Maximum optical power of laser diode	85 mW
Number of SPAD elements in a array	64
Photon detection probability	25%
Dead-time	5 ns
Average Dark Count rate	90 KHz
Photon Energy	4.42×10^{-19} J

To validate the effectiveness of our proposed deep learning aided signal detection scheme, two other schemes are utilized as two baselines. In the first scheme, after FFT operation with the received signal, the frequency-domain signal is obtained and be demodulated with the logarithmic likelihood ration (LLR) based soft-decision directly. In the scheme, this demodulation block is called as the LLR demodulator. While in the second scheme, a MLP network is combined with the LLR demodulator. This MLP network is only used for channel compensation to mitigate the distortion caused by the optical channel and SPAD. Its architecture is the same as that of the first subnetwork in the proposed scheme. Note that the light moving distance is used in the simulation instead of the signal-to-noise ratio. This is because the photons' interaction with the particles in the water lead to a complex relationship between the distance and the attenuation in UOWC. The impact of the distance is considered afterwards.

A. PERFORMANCE COMPARISON

Fig. 6(a)-(f) demonstrate the performance comparison of the proposed scheme with the two baseline on the received signals in different cases. Here, two channel models are considered to generate the received signals, namely the numerical optical channel model and the Beer Law model. Besides, the performance on AQ SPAD and PQ SPAD are also investigated. From these figures, it can be observed that the overall BER performance of the proposed scheme is better than the two baselines. The difference between the two baselines is that a deep learning network structure (also the first subnetwork of our proposed scheme) is utilized for channel compensation. With such network, the BER can be improved greatly. In our proposed scheme, the second subnetwork is adopted by replacing the LLR demodulator, which can be regarded as a fine-tuning process. Hence, the BER can be further improved with the prior knowledge of the original transmitted bits.

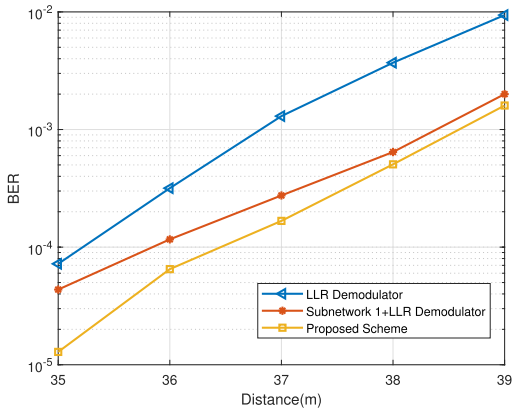

(a) Coastal Water, Numerial Optical Channel Model, AQ SPAD

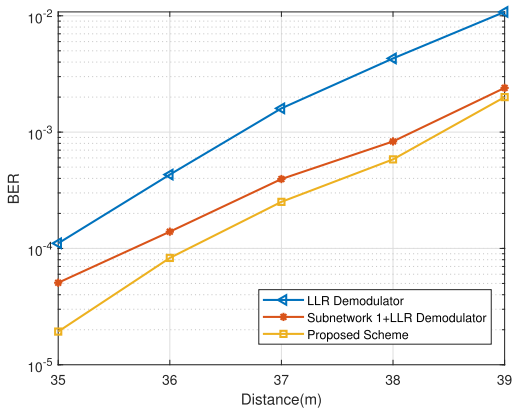

(b) Coastal Water, Numerial Optical Channel Model, PQ SPAD

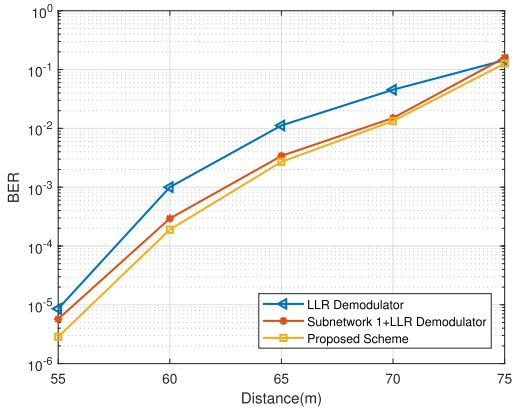

(c) Clear Ocean, Numerial Optical Channel Model, AQ SPAD

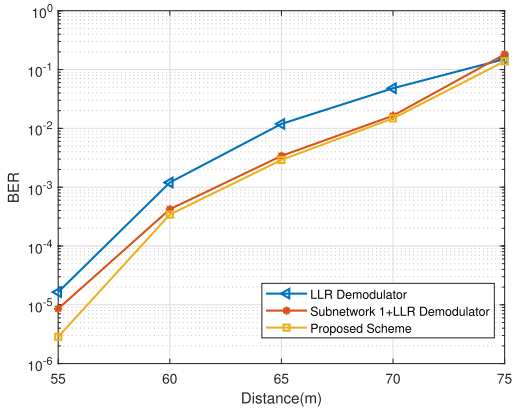

(d) Clear Ocean, Numerial Optical Channel Model, PQ SPAD

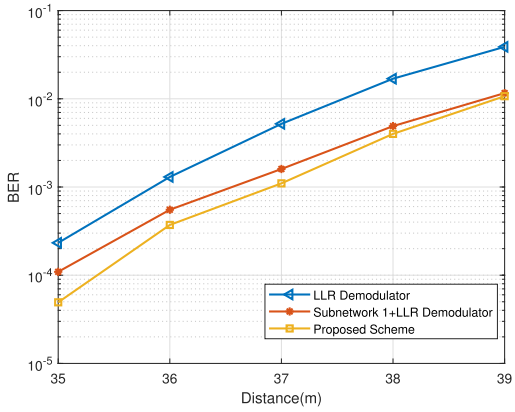

(e) Coastal Water, Beer Law Model, AQ SPAD

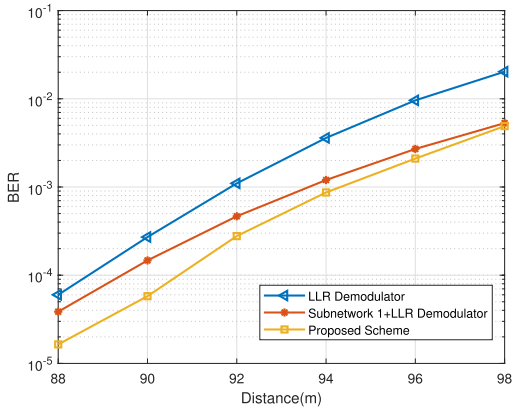

(f) Clear Ocean, Beer Law Model, AQ SPAD

FIGURE 6. **BER comparison on the received signals in different cases.**

1) COMPARISON OF WATER TYPES

In Fig. 6, the BER performance in the cases of different water types are compared. When using the proposed two-connected MLP network, for the clear ocean water type, the BER performance can be improved more in the relatively short distance than the long distance. This is because the data in the relative short distance suffers less distortion imposed by the channel and SPAD as well as the noise. The network can better extract the features of the received signals and recover the original information. On the contrary, in the relatively long distance, the data has extremely low power and is severely polluted by the non-Poisson-related noise and the

dark count noise. The deep learning network can no longer discern the received signal. The recovery of the information bits from such data would contribute to an extremely low BER. The performance is even worse than that of directly demodulating the signal. More importantly, it can be seen that the degree of the distance improvement in clear ocean water with the proposed scheme is higher than that in coastal water. Specifically, in consideration of the same BER target (below the forward error correction threshold), the improved distance can be extended up to 3 m in clear ocean water with the proposed scheme whereas the improvement is only 1.8 m for coastal water. This effect is caused by the light characteristics when travelling in different water. In the water with higher turbility, the optical channel would deteriorate rapidly even in a short distance. Accordingly, its BER would drop faster than in the clearer water and the proposed scheme could not further recover the transmitted information.

2) COMPARISON OF SPAD TYPES

The performance of the proposed scheme on different SPAD types are also investigated in Fig. 6. The two subfigures in the left column (Fig. 6(a)&(c)) are the simulation results for AQ SPAD while the two subfigures in the right column (Fig. 6(b)&(d)) are the results for PQ SAPD. It can be observed that there is a slightly difference between the impact on AQ SPAD and PQ SPAD, especially in the relatively short distance range. The achieved BER with the proposed scheme for AQ SPAD is better than PQ SPAD at the same distance. This is reasonable because the dead time would be extended by another photon arrival during the previous photon detection in PQ SPAD while the dead time of AQ SPAD retains constant. Therefore, the nonlinearity caused by PQ SPAD as well as the received signal is mildly worse than the AQ SPAD.

3) COMPARISON OF OPTICAL CHANNEL MODEL

As is illustrated in Fig. 6, the performance of the proposed scheme on the received signal generated with different optical channel models are studied. For fair comparison, their MLP network parameters are obtained with their own model-generating training data. An interesting result can be noticed from Fig. 6(a) & (e), which is the achieved BER is better for data generated with the numerical optical channel than the widely used Beer Law model for coastal water at the same distance. This occurs because a higher received signal power with the numerical channel model can be obtained compared to the Beer Law model where the scattering photons are assumed to be lost. On the other hand, from Fig. 6(c) & Fig. 6 (f), it can be seen that the distance where the proposed scheme is working for the data generated with the numerical optical channel model (i.e., smaller than 75 m) is smaller than the Beer Law model (i.e., larger than 88 m) in the clear ocean water case. This is supported by the fact that the beam spreading is considered in the numerical optical channel model, which causes the additional of optical power loss compared to the Beer Law model when the light propagates through a long distance. This would further cause the received power of Beer Law model is higher than the numerical optical channel model and lead to better received signals.

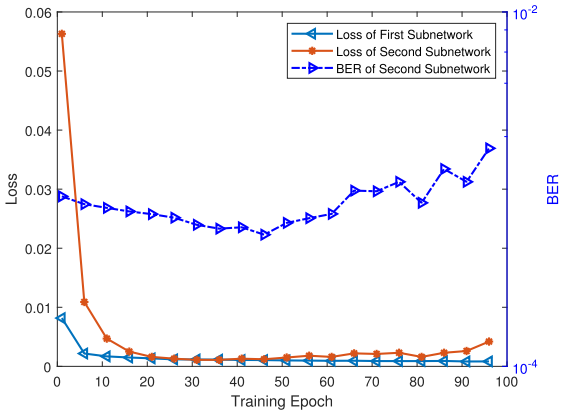

FIGURE 7. Performance comparison of each training epoch for the proposed network (Training data: coastal water, numerical optical channel model and AP SPAD model).

B. IMPACT OF TRAINING EPOCH

Finally, in Fig. 7, the impact of the training epoch on the loss function of the validation data and the BER performance of the two-connected network is evaluated. In this case, the water type is the coastal water and the training data is generated with the numerical optical channel model and AP SPAD model. Clearly, for the first subnetwork, as the epoch increases, the value of the loss function continuously decreases until a stead stable is obtained. However, the loss function of the second subnetwork firstly decreases and then slowly rises after the epoch increases to be 45, which is common (i.e., overfitting) in deep learning network. As a result, the overall BER trend of the output data of the second subnetwork goes up. To address this issue, the early stopping method (i.e., stopping the network training when a good result is obtained) is adopted in our simulation [32]. In addition, the loss as well as the BER goes up and down after the epoch reaches 65 in spite that the general trends of their values are climbing up. This is because in each epoch, the training data is randomly chosen from the dataset and the change of the data's quality determines the variations of the loss and BER.

V. CONCLUSION

In this paper, we propose a novel deep learning aided signal detection scheme for SPAD based UOWC system to deal with the distortion imposed by the underwater optical channel and SPAD. Compared to existing channel compensation or channel equalization methods, the channel side information is no longer needed for the proposed scheme. With the prior expert knowledge of the signal processing method, a two-connected MLP based deep learning network is adopted and embedded into the receiver. The first subnetwork is built for channel compensation while the second one works as a demodulator. Consequently, the two subnetworks are trained sequently with different loss functions. Besides, to train the proposed

network properly, vast training data for different water types are simulated with the numerical optical channel model and SPAD non-Poisson model. Simulation results show that the overall BER performance of the proposed scheme is better than two baselines. In addition, the degree of distance improvement in clear ocean water with the proposed scheme is better than that in coastal water as the optical channel would deteriorate rapidly for a short distance variation in coastal water.

REFERENCES

[1] J. G. Andrews, S. Buzzi, W. Choi, S. V. Hanly, A. Lozano, A. C. K. Soong, and J. Zhang, "What will 5G be," *IEEE J. Sel. Areas Commun.*, vol. 32, no. 6, pp. 1065–1082, Jun. 2014.

[2] X. Huang, J. A. Zhang, R. P. Liu, Y. J. Guo, and L. Hanzo, "Airplane-aided integrated networking for 6G wireless: Will it work?" *IEEE Veh. Technol. Mag.*, vol. 14, no. 3, pp. 84–91, Sep. 2019.

[3] Z. Zhang, Y. Xiao, Z. Ma, M. Xiao, Z. Ding, X. Lei, G. K. Karagiannidis, and P. Fan, "6G wireless networks: Vision, requirements, architecture, and key technologies," *IEEE Veh. Technol. Mag.*, vol. 14, no. 3, pp. 28–41, Sep. 2019.

[4] Z. Zeng, S. Fu, H. Zhang, Y. Dong, and J. Cheng, "A survey of underwater optical wireless communications," *IEEE Commun. Surveys Tuts.*, vol. 19, no. 1, pp. 204–238, 1st Quart., 2017.

[5] E. M. Sozer, M. Stojanovic, and J. G. Proakis, "Underwater acoustic networks," *IEEE J. Ocean. Eng.*, vol. 25, no. 1, pp. 72–83, Jan. 2000.

[6] X. Che, I. Wells, G. Dickers, P. Kear, and X. Gong, "Re-evaluation of RF electromagnetic communication in underwater sensor networks," *IEEE Commun. Mag.*, vol. 48, no. 12, pp. 143–151, Dec. 2010.

[7] X. Liu, S. Yi, X. Zhou, Z. Fang, Z.-J. Qiu, L. Hu, C. Cong, L. Zheng, R. Liu, and P. Tian, "345 m underwater optical wireless communication with 270 Gbps data rate based on a green laser diode with NRZ-OOK modulation," *Opt. Express*, vol. 25, no. 22, pp. 27937–27947, Oct. 2017.

[8] Y. Chen, M. Kong, T. Ali, J. Wang, R. Sarwar, J. Han, C. Guo, B. Sun, N. Deng, and J. Xu, "26 m/55 Gbps air-water optical wireless communication based on an OFDM-modulated 520-nm laser diode," *Opt. Express*, vol. 25, no. 13, pp. 14760–14765, Jun. 2017.

[9] L. Zhang, D. Chitnis, H. Chun, S. Rajbhandari, G. Faulkner, D. O'Brien, and S. Collins, "A comparison of APD- and SPAD-based receivers for visible light communications," *J. Lightw. Technol.*, vol. 36, no. 12, pp. 2435–2442, Jun. 15, 2018.

[10] E. Sarbazi, M. Safari, and H. Haas, "Statistical modeling of single-photon avalanche diode receivers for optical wireless communications," *IEEE Trans. Commun.*, vol. 66, no. 9, pp. 4043–4058, Sep. 2018.

[11] Z. Qin, H. Ye, G. Y. Li, and B.-H.-F. Juang, "Deep learning in physical layer communications," *IEEE Wireless Commun.*, vol. 26, no. 2, pp. 93–99, Apr. 2019.

[12] C. Zhang, P. Patras, and H. Haddadi, "Deep learning in mobile and wireless networking: A survey," *IEEE Commun. Surveys Tuts.*, vol. 21, no. 3, pp. 2224–2287, 3rd Quart., 2019.

[13] N. Chi, Y. Zhao, M. Shi, P. Zou, and X. Lu, "Gaussian kernel-aided deep neural network equalizer utilized in underwater PAM8 visible light communication system," *Opt. Express*, vol. 26, no. 20, pp. 26700–26712, Oct. 2018.

[14] P. Miao, B. Zhu, C. Qi, Y. Jin, and C. Lin, "A model-driven deep learning method for LED nonlinearity mitigation in OFDM-based optical communications," *IEEE Access*, vol. 7, pp. 71436–71446, 2019.

[15] H. Lee, I. Lee, T. Q. S. Quek, and S. H. Lee, "Binary signaling design for visible light communication: A deep learning framework," *Opt. Express*, vol. 26, no. 14, pp. 18131–18142, Jul. 2018.

[16] S. Ma, J. Dai, S. Lu, H. Li, H. Zhang, C. Du, and S. Li, "Signal demodulation with machine learning methods for physical layer visible light communications: Prototype platform, open dataset, and algorithms," *IEEE Access*, vol. 7, pp. 30588–30598, 2019.

[17] T. J. Petzold, "Volume scattering functions for selected ocean waters," Scripps Inst. Oceanogr., San Diego, CA, USA, Tech. Rep. SIO 7278, 1972.

[18] A. Sokolov, M. Chami, E. Dmitriev, and G. Khomenko, "Parameterization of volume scattering function of coastal waters based on the statistical approach," *Opt. Express*, vol. 18, no. 5, pp. 4615–4636, Mar. 2010.

[19] A. Laux, R. Billmers, L. Mullen, B. Concannon, J. Davis, J. Prentice, and V. Contarino, "The a, b, c s of oceanographic lidar predictions: A significant step toward closing the loop between theory and experiment," *J. Mod. Opt.*, vol. 49, nos. 3–4, pp. 439–451, Mar. 2002.

[20] L. C. Henyey and J. L. Greenstein, "Diffuse radiation in the galaxy," *Astrophys. J.*, vol. 93, pp. 70–83, Jan. 1941.

[21] V. I. Haltrin, "One-parameter two-term Henyey-Greenstein phase function for light scattering in seawater," *Appl. Opt.*, vol. 41, no. 6, pp. 1022–1028, Feb. 2002.

[22] G. R. Fournier and J. L. Forand, "Analytic phase function for ocean water," *Proc. SPIE*, vol. 2258, pp. 194–201, Oct. 1994.

[23] H. C. van de Hulst, *Multiple Light Scattering: Tables, Formulas, and Applications*. New York, NY, USA: Academic, 2012.

[24] C. Gabriel, M.-A. Khalighi, S. Bourennane, P. Léon, and V. Rigaud, "Monte-Carlo-based channel characterization for underwater optical communication systems," *J. Opt. Commun. Netw.*, vol. 5, no. 1, pp. 1–12, Jan. 2013.

[25] S. Tang, Y. Dong, and X. Zhang, "Impulse response modeling for underwater wireless optical communication links," *IEEE Trans. Commun.*, vol. 62, no. 1, pp. 226–234, Jan. 2014.

[26] Y. Zhang, J. Li, Y. V. Zakharov, J. Li, Y. Li, C. Lin, and X. Li, "Deep learning based single carrier communications over time-varying underwater acoustic channel," *IEEE Access*, vol. 8, pp. 38420–38430, 2019.

[27] A. Mousavi and R. G. Baraniuk, "Learning to invert: Signal recovery via deep convolutional networks," in *Proc. IEEE Int. Conf. Acoust., Speech Signal Process. (ICASSP)*, New Orleans, LA, USA, Mar. 2017, pp. 1–6.

[28] H. Ye, G. Y. Li, and B.-H. Juang, "Power of deep learning for channel estimation and signal detection in OFDM systems," *IEEE Wireless Commun. Lett.*, vol. 7, no. 1, pp. 114–117, Feb. 2018.

[29] W. Lyu, Z. Zhang, C. Jiao, K. Qin, and H. Zhang, "Performance evaluation of channel decoding with deep neural networks," in *Proc. IEEE Int. Conf. Commun. (ICC)*, Kansas City, MO, USA, May 2018, pp. 1–6.

[30] Q. Cheng, Z. Shi, D. N. Nguyen, and E. Dutkiewicz, "Sensing OFDM signal: A deep learning approach," *IEEE Trans. Commun.*, vol. 67, no. 11, pp. 7785–7798, Nov. 2019.

[31] S. Ioffe and C. Szegedy, "Batch normalization: Accelerating deep network training by reducing internal covariate shift," in *Proc. IEEE Int. Conf. Mach. Learn.*, Lille, France, Jul. 2015, pp. 448–456.

[32] I. Goodfellow, Y. Bengio, and A. Courville, *Deep Learning*. Cambridge, MA, USA: MIT Press, 2016.

[33] D. P. Kingma and J. Ba, "Adam: A method for stochastic optimization," in *Proc. Int. Conf. Learn. Represent.*, San Diego, CA, USA, May 2015, pp. 1–15.

RUI JIANG received the B.E. and M.E. degrees from Beijing Jiaotong University, Beijing, China, in 2011 and 2014, respectively, and the Ph.D. degree in electronic engineering from Tsinghua University, Beijing, in 2018. He is currently a Research Assistant Professor with Peng Cheng Laboratory (PCL), Shenzhen, China. His research interests include optical wireless communications, digital signal processing, machine learning, and optimization theory.

CAIMING SUN received the B.S. and M.S. degrees from Beijing Normal University, Beijing, China, in 2002 and 2005, respectively, and the Ph.D. degree in electronic engineering from The Chinese University of Hong Kong (CUHK), Hong Kong, in 2008. He has more than ten years of R&D experience, supported by Hong Kong Innovation and Technology Funds, working on optical communications, nanophotonics, nanofabrication, and wearable electronics. He is currently a Researcher with the Institute of Robotics and Intelligent Manufacturing (IRIM), The Chinese University of Hong Kong (CUHK), Shenzhen, China, and an Associate Professor with the Robotics Research Center, Peng Cheng Laboratory (PCL), Shenzhen. His research interests include LiDAR technologies for robotics, underwater wireless optical communications, and Si photonics.

LONG ZHANG received the master's degree in wireless communications from the University of Southampton, in 2012, and the Ph.D. degree in engineering science from the University of Oxford, in 2019. He is currently a Research Assistant Professor with the Peng Cheng Laboratory. His current research interests include optical wireless communication systems, wireless signal processing, and optical receiver design.

XINKE TANG received the M.Res. and Ph.D. degrees from the University of Cambridge, Cambridge, U.K., in 2014 and 2019, respectively. He is currently an Assistant Researcher with the Robotics Research Center, Peng Cheng Laboratory. His research interests include underwater optical wireless communication, optical networks, optical switching, and quantum key distribution.

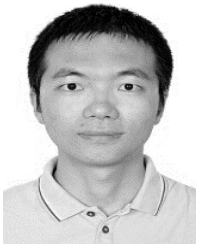

HONGJIE WANG was born in Hubei, China, in September 1986. He received the bachelor's degree in optoelectronic from the Huazhong University of Science and Technology, China, the M.S. degree in optical sciences from Rouen University, in 2012, and the Ph.D. degree from Rouen University, in 2017. He was a Graduated Engineer in the area of electronics from ESIGELEC, Rouen, France. Since 2018, he has been a Postdoctoral Researcher with The Chinese University of Hong Kong, Shenzhen. His research interests include high power fibre laser optical communication systems and silicon-photonics chips.

AIDONG ZHANG received the B.S. and Ph.D. degrees in computer science from Zhejiang University, Hangzhou, China, in 1991 and 1996, respectively. From 1996 to 2015, he was the Vice General Manager of the Multimedia Business Unit, the Director of the Research and Development Cooperate Department, and the Director of the Media and Communication Laboratory, Huawei Technologies Company, Ltd., Shenzhen, China. Since 2016, he has been the Director of the Institute of Robotics and Intelligent Manufacturing (IRIM), The Chinese University of Hong Kong (CUHK), Shenzhen. He is also the Director of the Robotics Research Center, Peng Cheng Laboratory (PCL), Shenzhen, and the Vice President of the Shenzhen Institute of Artificial Intelligence and Robotics for Society (AIRS), Shenzhen. His current research interests include media and communication, robotics, computer vision, virtual reality, and the Internet of Things. He was a recipient of the National Science and Technology Progress Award, China, in 2012.